AIAA 91-0728

# FLU3PNS : A THREE-DIMENSIONAL THIN LAYER AND PARABOLIZED NAVIER-STOKES SOLVER USING THE MUSCL UPWIND SCHEME

Eric CHAPUT, François DUBOIS
AEROSPATIALE, Space and Strategic Systems Division,
BP 96, F-78133, Les Mureaux cedex, France,

Didier LEMAIRE , Gilles MOULES
SEGIME, 142 rue Pierre Curie, 78130 Les Mureaux, France,

Jean Louis VAUDESCAL
AEROSPATIALE, Space and Strategic Systems Division,
BP 96, F-78133, Les Mureaux cedex, France.

**29th Aerospace Sciences Meeting**
January 7-10, 1991/Reno, Nevada

# FLU3PNS : A THREE-DIMENSIONAL THIN LAYER AND PARABOLIZED NAVIER-STOKES SOLVER USING THE MUSCL UPWIND SCHEME.

Eric CHAPUT *, François DUBOIS **,
AEROSPATIALE, Space and Strategic Systems Division,
BP 96, F-78133, Les Mureaux cedex, France,

Didier LEMAIRE *, Gilles MOULES *,
SEGIME, 142 rue Pierre Curie, 78130 Les Mureaux, France,

Jean Louis VAUDESCAL †
AEROSPATIALE, Space and Strategic Systems Division,
BP 96, F-78133, Les Mureaux cedex, France.

**Abstract**

The operational Euler code FLU3C developed at the Office National d'Etudes et de Recherches Aérospatiales and at Aerospatiale Tactical Missiles Division has been extended at Aerospatiale Space and Strategic Systems Division to take into account viscous effects that are dominant in hypersonic regimes. Two different approximations of the compressible Navier-Stokes equations, namely the unsteady Thin Layer and Parabolized Navier-Stokes Equations are integrated numerically in time with the second order accurate MUSCL upwind scheme for the inviscid fluxes and a centered scheme for the viscous effects. The algorithm remains of space-marching type in the PNS case due to the parabolic nature of the partial differential equation and a "plane by plane" algorithm. Vigneron's stability condition for the PNS case is treated in conservative form. The numerical viscosity has been reduced by using Osher's approximate Riemann Solver. The computer code proves its capability to compute classical flows such as supersonic flat plates and sphere-cones. With the TLNS version it is also used to predict flows where subsonic pockets are present such as ramp flows. Three-dimensional geometries such as delta wing and the European space shuttle Hermes are also presented.

## I Introduction

The design of hypersonic vehicles requires the development of high level CFD computer codes to provide reliable prediction of aerodynamic coefficients in flight conditions. They must include both precise geometrical representation and appropriate physical modeling in order to reach a similitude not available with wind tunnels tests. Compressibility effects are described by the Euler equations of gas dynamics and are sufficient to represent essential phenomena like the detached shock wave (blunt body body configuration), oblique shock waves with rotational effects, rarefaction fans, etc... Secondly, the introduction of viscous effects are essential for prediction of skin friction and heat flux coefficients. This can be done in weak interaction regimes from an Euler solver via coupling with a boundary layer code. But in the regions of strong interaction (blunt nose, regions with recirculating flow, base flow), the Complete Navier-Stokes (CNS) equations have to be solved. Moreover, complex physical models (turbulence, real gases including chemistry effects, rarefied flows at high altitudes) also have to be considered for complete physical modeling. However the computation of numerical solutions of the CNS equations remains too expensive for the prediction of viscous flows in all industrial configurations. Two approximations of the CNS equations are studied in this paper : the Thin Layer Navier Stokes (TLNS) and Parabolized Navier Stokes (PNS) equations. With these approximations it is possible to describe complex interaction domains such as streamwise separating flows (TLNS approximation) and recirculating flows in the crosswise direction (PNS approximation).

Classically, the PNS equations are associated with a stationary formulation of the conservation laws of gas dynamics [1] and are solved numerically with a centered scheme and a space marching algorithm with a shock fitting procedure [2, 3, 4]. During the last years, the stationary approach has been adapted to second order accurate upwind schemes [5, 6, 7]. On the other hand, the introduction of viscous fluxes in a time marching Euler solver is natural for integrating the TLNS equations [8, 9]. Our computer code is based on this last approach : the industrial code FLU3C [10, 11] based on an upwind centered numerical scheme and a time marching algorithm has been extended to the TLNS and PNS equations in a way proposed by Chang-Merkle [12] (see also [13, 14]). The PNS equations are considered as unstationary equations and the space marching results is coupled with a time marching approach in each plane.

## II Finite volume formulation of the governing equations

We discretize the instationary CNS equations of a polytropic perfect gas with the finite volume method on a structured mesh. The conservative variables $U_{ijk}$ at a

---

* Research Engineer, Aerodynamics Department

** Research Engineer, Applied Mathematics Department, Member AIAA

† Graduate Student

mesh vertex $x_{ijk}$ are considered as mean values in the associated control volume $V_{ijk}$. They are incremented between times $n\Delta t$ and $(n+1)\Delta t$ thanks to the conservation laws of mass, momentum and energy integrated in $V_{ijk}$ :

$$\frac{1}{\Delta t}\left(U^{n+1}_{i,j,k} - U^{n}_{i,j,k}\right) + \tag{1}$$

$$+\frac{1}{|V_{ijk}|}\int_{\partial V_{ijk}} \left\{ (f\cdot n)^{inviscid} + (f\cdot n)^{viscous} \right\} d\gamma = 0 \ .$$

The construction of $V_{ijk}$ and the normal vectors n to the boundaries $\partial V_{ijk}$ are detailed in Ref. 11 and included references. We point out that the CNS equations are discretized in the physical space (finite volumes) without any transformation of coordinates.

**TLNS and PNS approximations of the viscous fluxes.**

In the following, we assume that the k-direction corresponds to the marching direction of the flow. The main approximation of both TLNS and PNS is of neglecting the viscous fluxes in this direction :

$$(f\cdot n)^{viscous}_{i,j,k+1/2} = 0 \ . \tag{2}$$

The other fluxes $(f\cdot n)_{i+1/2,j,k}{}^{viscous}$ and $(f\cdot n)_{i,j+1/2,k}{}^{viscous}$ are classical [15] functions of the gradients $\nabla u$ and $\nabla T$ of velocity and temperature at the associated interface. We detail the evaluation of the gradient $\nabla u_{i+1/2,j,k}$ ; the generalization to other cases is straightforward. Following [16], we introduce a "shifted cell" $\Omega_{i+1/2,j,k}$ whose boundary is composed by six faces that are naturally associated with the following indices (see Figure 1) :

$$\partial\Omega_{i+1/2,j,k} : \ (i,j,k),\ (i+1,j,k),\ (i+1/2,j,k+1/2),$$
$$(i+1/2,j,k-1/2),\ (i+1/2,j+1/2,k),\ (i+1/2,j-1/2,k) \ . \tag{3}$$

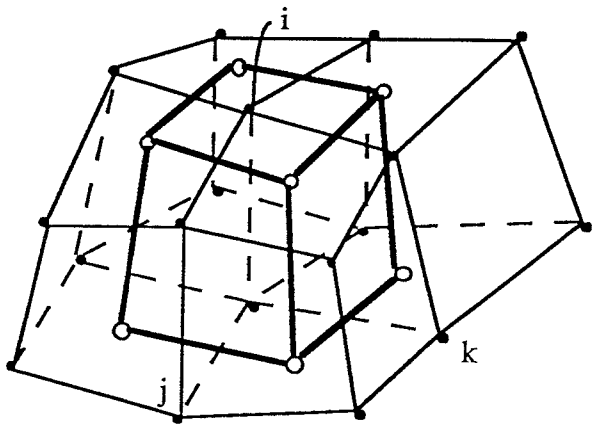


Figure 1. Shifted cell $\Omega_{i+1/2,j,k}$ for the evaluation of interface gradients.

The gradient at the interface (i+1/2,j,k) is computed according to Green's formula :

$$\nabla u_{i+1/2,j,k} = \frac{1}{|\Omega_{i+1/2,j,k}|}\int_{\partial\Omega_{i+1/2,j,k}} \tilde{u}\cdot n \ d\gamma \tag{4}$$

and the viscous scheme is entirely defined by the way we interpolate u in the right hand side of (4). For each face of $\partial\Omega_{i+1/2,j,k}$ defined in (3), we first introduce interpolated values of the conservative variables as follows :

$$\tilde{U}_{i,j,k} = U_{i,j,k} \tag{5}$$

$$\tilde{U}_{i+1/2,j+1/2,k} = \frac{1}{4}\left( U_{i,j,k} + U_{i+1,j,k} + \right.$$
$$\left. + U_{i+1,j+1,k} + U_{i,j+1,k} \right) \tag{6}$$

For the k-faces, we consider two sub-cases :

$$\text{TLNS} : \tilde{U}_{i+1/2,j,k+1/2} = \frac{1}{4}\left( U_{i,j,k} + U_{i+1,j,k} + \right.$$
$$\left. + U_{i+1,j,k+1} + U_{i,j,k+1} \right) \tag{7}$$

$$\text{PNS} : \tilde{U}_{i+1/2,j,k+1/2} = \frac{1}{2}\left( U_{i,j,k} + U_{i+1,j,k} \right). \tag{8}$$

Therefore in the PNS case the viscous fluxes associated with cells $V_{ijK}$ in the plane k=K are only functions of the variables $U_{ijK}$ in the same computing plane. Then we deduce velocity and temperature from these conservative variables on each face of the shifted cell $\partial\Omega_{i+1/2,j,k}$ and apply relation (4) to compute the gradients in the viscous fluxes. Note also that the viscosity is assumed to be only a function of temperature ; for each interface of the control volume $V_{ijk}$ , we interpolate the temperature field then compute viscosity and thermal conductivity (a constant Prandtl number is assumed).

**MUSCL Scheme for the inviscid fluxes**

The general principles concerning the second order accurate MUSCL approximation of the inviscid fluxes related to the conservation laws have been proposed by Van Leer [17]. We recall the choices made in the FLU3C computer code. The scheme is second order accurate in time, of predictor-corrector type. We introduce the so-called primitive variables

$$W = (\rho\ ,\mathbf{u}\ ,p)\ ,\ \left(U = (\rho\ ,\rho\mathbf{u}\ ,\rho\frac{|\mathbf{u}|^2}{2} + \rho\, e)\right) \tag{9}$$

at time $t^n$ and node $x_{ijk}$. Then nonlinear interpolated values along mesh directions are defined as follows (we detail only the evaluation of $W_{i+1/2,j,k}{}^{-}$ in the i-direction) :

$$\overline{W}_{i,j,k} = \frac{1}{10}\left(W_{i,j,k} + \sum_{l,\,m\,=\,-1,0,+1} W_{i,j+l,k+m}\right) \tag{10}$$

$$\delta\bar{W}^{\pm}_{i,j,k} = \pm \left( \bar{W}_{i\pm1,j,k} - \bar{W}_{i,j,k} \right) \qquad (11)$$

$$W^{-}_{i+1/2,j,k} = W_{i,j,k} + \frac{\left((\delta\bar{W}^{-}_{i,j,k})^2 + \varepsilon\right) \delta\bar{W}^{+}_{i,j,k} + \left((\delta\bar{W}^{+}_{i,j,k})^2 + \varepsilon\right) \delta\bar{W}^{-}_{i,j,k}}{2\left[ (\delta\bar{W}^{+}_{i,j,k})^2 + (\delta\bar{W}^{-}_{i,j,k})^2 + 2\,\varepsilon \right]} \qquad (12)$$

where

$$\varepsilon = 10^{-40} \qquad (13)$$

is the classical parameter of the Van Albada [18] limiter. Then, after elementary algebra, the gradient of the conservative variables is computed from the extrapolated values

$$U^{-}_{i+1/2,j,k}\ ,\ U^{+}_{i-1/2,j,k}\ ,\ U^{-}_{i,j+1/2,k}\ ,\ U^{+}_{i,j-1/2,k}\ ,\ U^{-}_{i,j,k+1/2}\ ,\ U^{+}_{i,j,k-1/2}\ . \qquad (14)$$

The predictor step is non-conservative :

$$\frac{1}{\Delta t / 2}\left( U^{n+1/2}_{i,j,k} - U^{n}_{i,j,k} \right) + \frac{1}{\left| V_{i,j,k} \right|} d f^{\,\mathrm{Euler}}(U^{n}_{i,j,k}) \bullet \nabla U^{n}_{i,j,k} = 0\ . \qquad (15)$$

The extrapolated values (14) are incremented in time according to the predictor step (15). The primitive variables at the interface are deduced ; for example, we have :

$$W^{n+1/2\,,-}_{i+1/2,j,k} = W^{-}_{i+1/2,j,k} + \left( W^{n+1/2}_{i,j,k} - W^{n}_{i,j,k} \right) \qquad (16)$$

$$W^{n+1/2\,,+}_{i+1/2,j,k} = W^{+}_{i+1/2,j,k} + \left( W^{n+1/2}_{i+1,j,k} - W^{n}_{i+1,j,k} \right). \qquad (17)$$

The conservative variables at each interface and time step $(n+1/2)\Delta t$ follow easily from (16)-(17). The result of the corrector step defines the inviscid flux of relation (1). It is obtained by an approximate solution of the monodimensional Riemann problem associated with a polytropic perfect gas ($\gamma = 1.4$) at the interface between two neighboring cells, along the normal direction. For the (i+1/2,j,k) interface we have :

$$(f\bullet n)^{\mathrm{inviscid}}_{i+1/2,j,k} = \Phi\left( U^{n+1/2,\,-}_{i+1/2,j,k}\ ,\ U^{n+1/2,\,+}_{i+1/2,j,k}\ ,\ n_{i+1/2,j,k} \right)\ . \qquad (18)$$

In the FLU3C computer code, the numerical flux $\Phi$ is the Van Leer [19] flux vector splitting. Since the work of Van Leer et al [20], it is well known that this flux is incompatible with an extension to viscous effects. Consequently, this flux has been replaced by Osher's approximate Riemann solver [21] which has the advantage of capturing all the compressible nonlinear waves (shock waves are simply replaced by multivalued rarefactions) and does not need any tuning parameter which is not the case for Roe's [22] solver used previously in the PNS codes with upwinding schemes.

**Inviscid fluxes for the PNS code.**

The algorithm of the previous section is applied without any modification when we integrate the TLNS equations. In the PNS case, we have to maintain the k-direction as a marching one. If the nodal values $U_{i+1/2,j,k}$ are known for $k \le K$ we first define extrapolated values in the plane k=K+1 according to :

$$U_{i,j,K+1} = U_{i,j,K} + \frac{1}{2}\left( U_{i,j,K} - U_{i,j,K-1} \right)\ . \qquad (19)$$

Then fluxes at interfaces (i+1/2,j,K) and (i,j+1/2,K) of the computing plane k=K are given according to the relations (11)-(18). In the marching direction, we consider the predicted states given by (15) and we define :

$$(f\bullet n)^{\mathrm{inviscid}}_{i,j,k+1/2} = (f\bullet n)^{\,\mathrm{Euler}}\left( U^{n+1/2}_{i,j,k+1/2} \right) - (1 - \omega^{n+1/2}_{i,j,k+1/2})\ (0\ ,\ p^{n+1/2}_{i,j,k+1/2}\,n\ ,\ 0\ )^{T} \qquad (20)$$

where $p_{i,j,k+1/2}$ is the pressure at the interface (i,j,k+1/2) and $\omega_{i,j,k+1/2}$ the Vigneron coefficient. We emphasize that in the present formulation the coefficient $\omega_{i,j,k+1/2}$ is associated with the interface (i,j,k+1/2) in order to maintain the conservative nature of the numerical scheme. The algebraic expression of $\omega_{i,j,k+1/2}$ is classical (see Ref. 3) and we have :

$$\omega_{i,j,k+1/2} = \min\left( 1, \frac{\sigma\gamma\, M_z^2(U_{i,j,k+1/2})}{1 + (\gamma-1)\, M_z^2(U_{i,j,k+1/2})} \right) \qquad (21)$$

where $M_Z$ is the ratio between the normal velocity at the interface and the associated sound velocity, $\gamma$ the ratio of specific heats and $\sigma$ a safety factor equal to 0.85.

With this approach, independently proposed by Chang-Merkle (Ref. 12), the PNS approximation is embedded into a general unstationary formulation of the partial differential equations witch gives an important flexibility concerning the algorithm for the numerical resolution.

**Boundary conditions**

We have implemented a classical no-slip boundary condition on the body in a simple way. We first note that the nodes $x_{ijk}$ of the mesh that define the center of the control volumes $V_{ijk}$ are defined on the surface of the body with our mesh generator (Figure 2). Therefore there is a priori no control volume well defined in the fluid

around the nodes located on the boundary ; the conservative unknowns $U_{ijk}$ for these nodes are not computed according to the relation (1) but directly with the Dirichlet boundary condition. We assume that the velocity and the temperature are given on the body ; we compute the pressure by an extrapolation from the neighboring node :

$$p^{n+1}_{i,j,k} = p^{n+1}_{i+1,j,k} \ , \quad x_{i,j,k} \text{ on the body} \qquad (22)$$

and the field $U_{ijk}$ is entirely known. At the fluid boundaries, we neglect the viscous effects and apply the Euler boundary conditions.

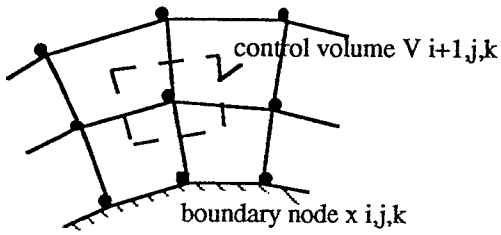


Figure 2. Boundary conditions.

### Temporal scheme

There is no major difference with the Euler code : the scheme is explicit, second order accurate in time for the inviscid fluxes (predictor-corrector type) and first order accurate in time for the viscous fluxes in the present version (the viscous fluxes are evaluated only at the corrector step). The time step is limited by a classical CFL condition as in Ref. 11.

### Initialization of the PNS version

The initialization of a PNS flow solver is a general and relatively difficult problem : we use the self-consistent "step back" technique [23] (see also [24]) or the TLNS version of the computer code. For blunt body configurations we initialize FLU3PNS by a complete Navier-Stokes solver [25].

### "Plane by plane" space marching algorithm

The "plane by plane" strategy of the algorithm (i.e. for marching in space, march in time) is one of the main points concerning the industrial efficiency of the Euler solver FLU3C. There is no major adaptation needed for extending the algorithm to the PNS equations (the TLNS are integrated globally in time via a classical time marching algorithm). We recall the main ideas of this algorithm.

We assume that all the variables $U_{ijk}$ are known in the "plane" k=K-1. Then we integrate in time the conservation law (1) in a localized spatial domain composed of the cells $V_{ijk}$ that satisfy k=K. The parabolic nature of the PNS equations ensures that the inviscid flux (20) at the interface K+1/2 is only a function of the variables $U_{ijk}$ for k=K-1 and k=K. Therefore all the fluxes are only functions of the data $U_{ijk}$ for k=K-1 and of the unknowns $U_{ijk}$ for k=K. This instationary algorithm is integrated until convergence in time is obtained. Then we march in space and change K into K+1.

## III Applications

The numerical method has been implemented on the Cray XMP 116 computer located at Aerospatiale, Les Mureaux. The computer code FLU3PNS is vectorized and the present performance with the explicit scheme is 40 micro-second per cell and per time step.

### Flat plate

The first test case consists of a supersonic laminar flow over a flat plate. The freestream conditions are the following ones :

$$M_\infty = 2, \ Re_\infty / L = 1.65\ 10^6 \ , \ L = 1 \text{ m}$$
$$Pr = 0.72, \ T_{wall} = T_\infty = 222 \text{ K} \ . \qquad (23)$$

The mesh contains 51 nodes in the direction normal to the plate and 54 in the marching direction. In the first box region ($0 \le x/L \le 0.3$) we integrate the TLNS equations. Then in the second box ($0.3 \le x/L \le 0.93$) we solve the PNS equations with a plane by plane space marching. We observe that FLU3PNS is self-initializing for this problem thanks to a coupling of the TLNS and PNS versions. Figures 3 and 4 display the variation of tangential velocity and temperature along the normal direction for z = 0.93 L, compared with the boundary layer code BA 99 [26]. On Figure 5, we present the normal gradient of the temperature with the help of the conventional heat flux. Recall that skin friction Cf and heat flux Ch coefficients are defined as follows :

$$C_f = \frac{(f \cdot n)^{\text{viscous}}_{\text{impulsion}}}{\frac{1}{2} \rho_\infty u_\infty^2} \ ,$$
$$C_h = \frac{\text{heat flux on the boundary}}{\rho_\infty u_\infty c_{p\infty} \left( (1 + \frac{\gamma - 1}{2} M_\infty^2) T_\infty - T_{wall} \right)} \ . \qquad (24)$$

We observe a good agreement with the boundary layer code and previous results of Refs. 5 and 7.

### Slender cone

The second test case simulates a three-dimensional laminar hypersonic flow over a cone of lengh L = 0.325 m with a 10° half angle at a 24° angle of attack freestream flow. The exact flow conditions are :

$$M_\infty = 7.95, \ Re_\infty = 4.101\ 10^6 \text{ m}^{-1} \ , \ L = 0.325 \text{ m} \ ,$$
$$\alpha = 24 \ °, \ Pr = 0.72, \ T_{wall} = 309.8 \text{ K}, \ T_\infty = 55.4 \text{ K} \ . \qquad (25)$$

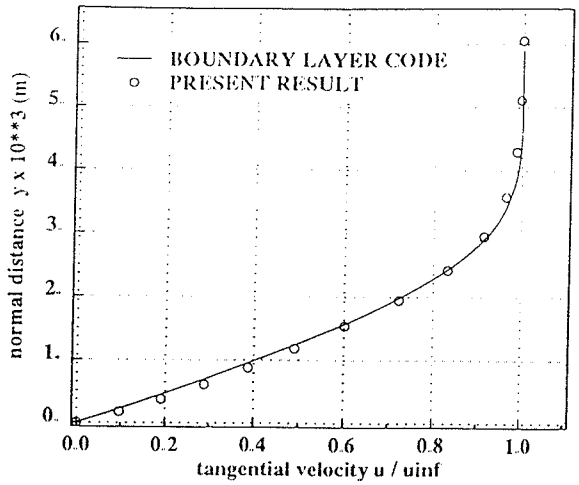


Figure 3. Flat plate. Tangential velocity profile.

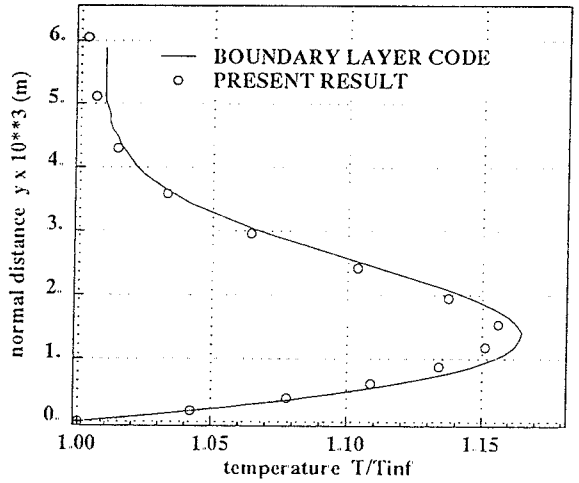


Figure 4. Flat plate. Temperature profile.

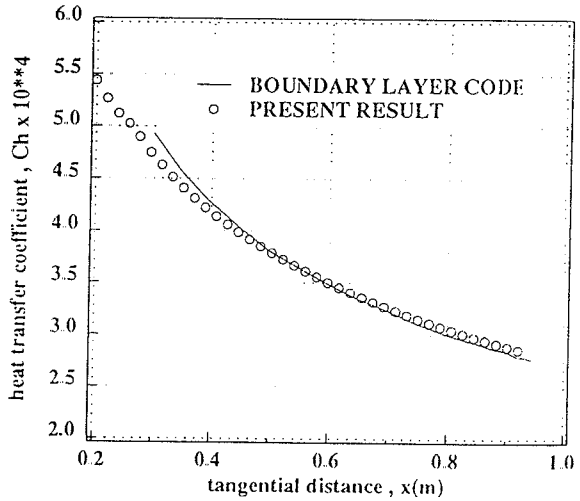


Figure 5. Heat transfer coefficient along the flat plate.

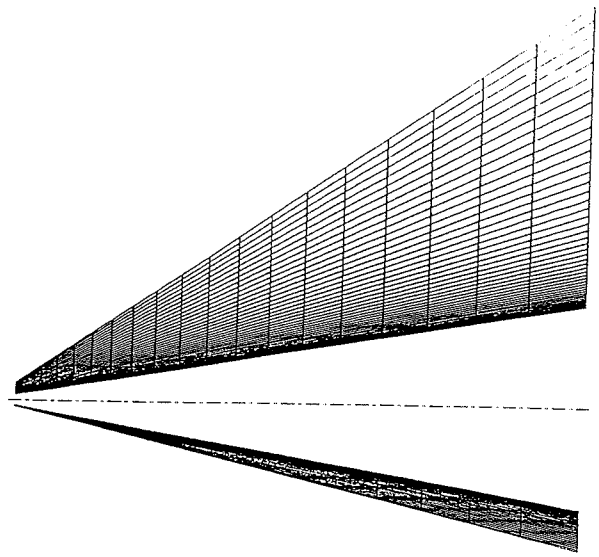

Figure 6. Slender cone. View of the mesh in the meridian plane.

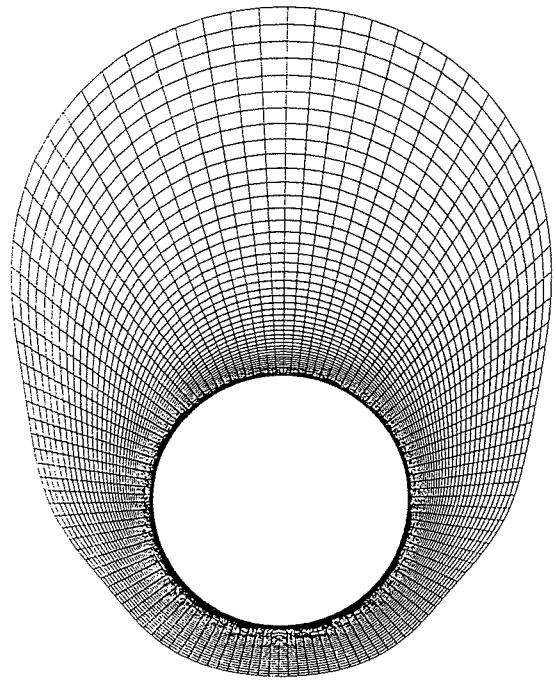

Figure 7. Slender cone. Mesh in a plane of space marching.

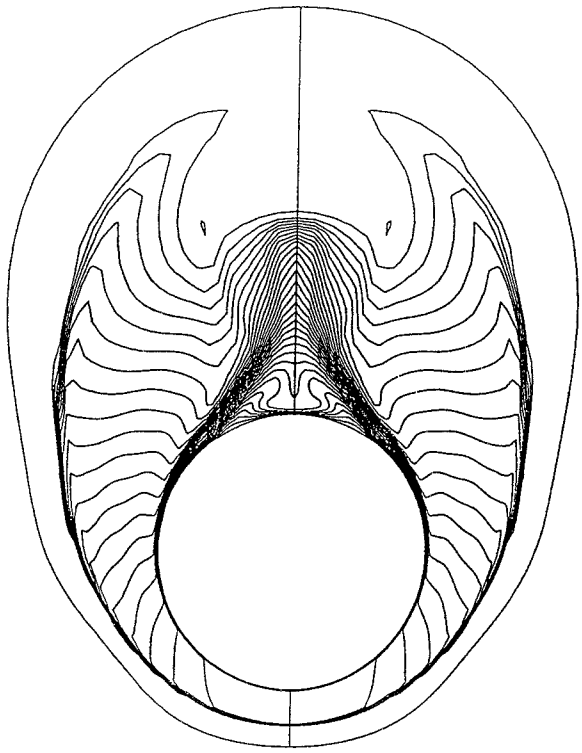

Figure 8. Slender cone. Iso-Mach contours in plane z = 0.266 (Δm = 0.25).

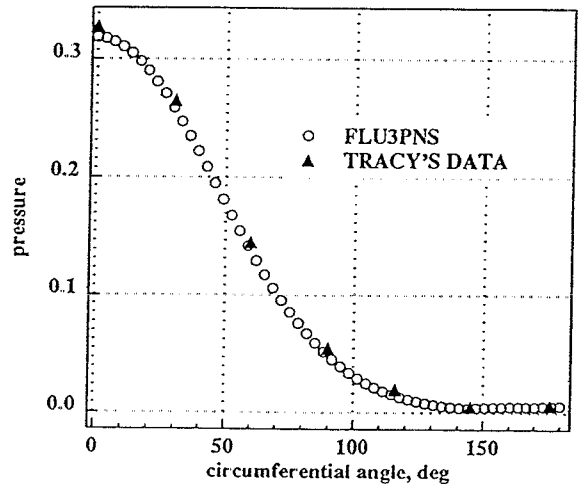


Figure 9. Pressure on the slender cone surface at z = 0.325 m.

The previous boundary conditions have been considered in Tracy's experiments [27]. The structure of the flow field is detailed in Ref. 7. The computational grid (Figures 6 and 7) contains 20 planes in the stream direction, 56 nodes between the leeward and windward sides and 51 nodes between the body and the external boundary. The computation has been initialized with the step back algorithm between planes 1 and 2 until convergence on these two planes. The iso-Mach contours are presented on Figure 8 at the location z = 0.266 m and are in good agreement with Figure 12 of Ref. 7. The bow shock is well captured as well as the crossflow separation. On Figure 9, we compare the pressure distribution on the body at x = 0.325 m and Tracy's data (Ref. 27).

**Flow over a two-dimensional wedge**

The third problem is a purely TLNS case : the hypersonic laminar flow over a 24° ramp experimentally studied by Holden and Moselle [28] is presented. A two-dimensional mesh of 87 nodes along the flow direction and 51 in the normal direction is used (Figure 10). The planes are equally spaced on the plate (45 points) and on the beginning of the ramp ($1 \leq x/L \leq 1.5$). Then a streching parameter equal to 1.06 is used for the 18 last planes. In the direction normal to the boundary a streching of 1.06 is also used. The freestream conditions are :

$$M_\infty = 14.1,\ Re_\infty / L = 104\ 10^3\ ,\ L = 0.439\ m\ ,$$
$$\beta_{ramp} = 24\ °,\ Pr = 0.72,\ T_{wall} = 297\ K,\ T_\infty = 72.2\ K\ . \quad (26)$$

The run is carried out in two steps : the first box ($-0.092 \leq x/L \leq 0.41$) is converged using the thin layer approximation. Then the same approximate equations are integrated in a second domain ($x/L \geq 0.41$). The total run requires 11 000 time steps. We emphasize on the importance of using a sufficiently refined mesh for capturing correctly the flow field. With the present 87x51 mesh, our results are in good agreement with Holden's data (see Figure 11 the iso-Mach contours). On Figures 12-14, the wall values of pressure, skin friction and heat flux are compared along the wedge. The recirculating zone is well captured with the TLNS version of the computer code. The pick of heat flux at the reattachment is particularily well predicted.

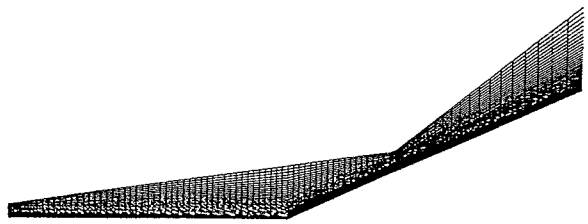

Figure 10. Mesh for the 2D ramp.

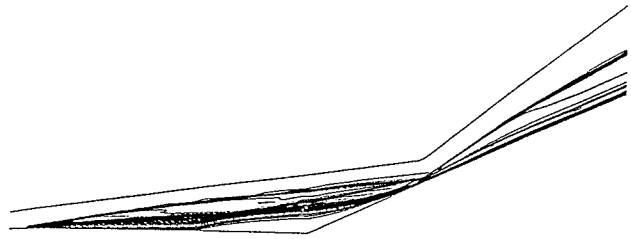

Figure 11. Iso-Mach contours for the 2D ramp (Δm = 0.5).

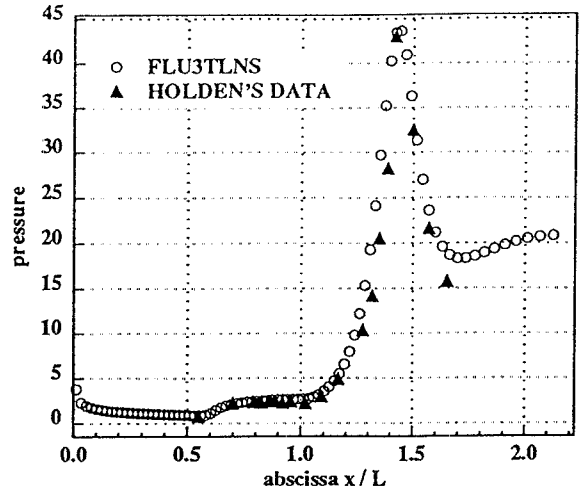


Figure 12. Pressure on the wall (2D ramp).

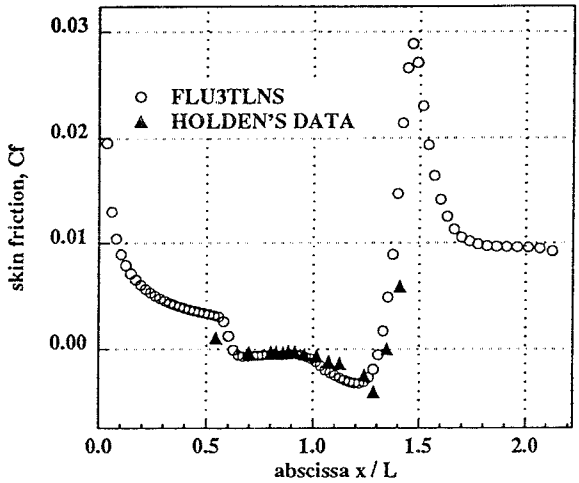


Figure 13 Skin friction (2D ramp).

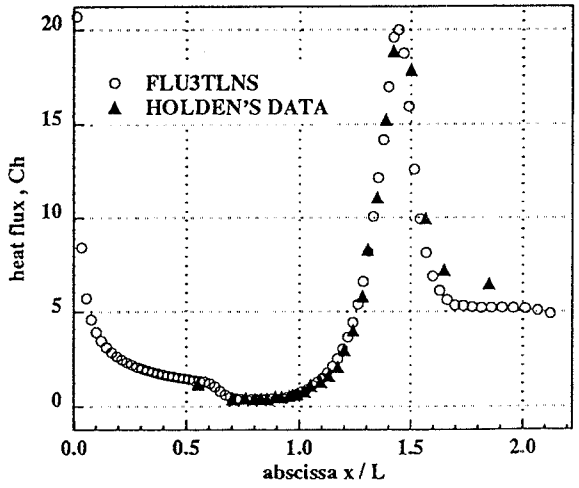


Figure 14 Heat flux (2D ramp).

**Delta wing**

The fourth test case is a delta wing proposed by the organisers of the Workshop on Hypersonic Flows for Reentry Problems [29]. The three-dimensional geometry is defined in Figure 15. The freestream and wall conditions are

$$M_\infty = 7.15,\ Re_\infty = 39\ 10^6\ m^{-1}\ ,\ L = 0.150\ m\ ,$$
$$\alpha = 30°\ ,\ Pr = 0.72,\ T_{wall} = 288\ K,\ T_\infty = 74\ K\ . \quad (27)$$

Initialization is obtained in the plane $z/L = 0.038$ (corresponding to the end of the plate region in the leeward side of the wing) with a step-back algorithm. Due to the a priori non-conical property of the flow field, several tests have been undertaken to ensure that the flow is well initialized by this procedure (different positions for the first two planes have been tested and the mesh has been refined). No definitive conclusion can be drawn, and a complete three-dimensional computation in the nose region would be necessary. We think that the initial profile of the boundary layer is fair. Between the nose region and the final section ($x/L = 0.5$) the computational domain is divided into 4 boxes (Figure 16) without a priori node coincidence. Two meshes have been generated and we display in Figure 17 the two-dimensional meshes in the final section (66x40 for the coarse mesh, 130x61 for the refined one). The four boxes of the fine mesh contains a total of 358522 nodes. The total run requires 5 hours on Cray XMP, which can be compared with the 18 hours on Cray 2 associated with a complete Navier Stokes solution on a 33x97x97 mesh proposed by Murman in Ref. 29. The iso-Mach contours in the plane $z/L = 0.5$ on the coarse and refined meshes are presented in Figure 18. They are in good agreement with previous results on the same test case presented by Rizzi and Chakravarthy in Ref. 29. We note also a sensible difference with other results of Ref. 29 on a very fine mesh. In Figure 19, the pressure field on the body is compared with two CNS results and in Figure 20, a detailed view shows agreement of the pressure on the leeward side of the wing with the experiments of Linde (see Ref. 29). The heat flux is compared in Figure 21 with Rizzi's results on a fine (33x129x97) mesh. The comparison is relatively fair but we think that our mesh has to be refined in cross-flow direction.

**Hermes European Space Shuttle**

We end this section concerning applications of FLU3PNS with a first industrial application on the Hermes 0.0 space plane. This computation, which includes both the space plane and its wake, has been achieved by coupling the computer codes HOMARD3 (a CNS solver, see Ref. 25) and FLU3PNS. The boundary conditions of this computation are the following ones :

$$M_\infty = 20\ (z = 70\ km)\ ,\ \alpha = 30°\ ,\ Re_\infty = 36\ 000\ m^{-1}\ ,$$
$$Pr = 0.72\ ,\ T_{wall} = 1000\ K\ ,T_\infty = 220\ K\ ,\ \gamma = 1.4. \quad (28)$$

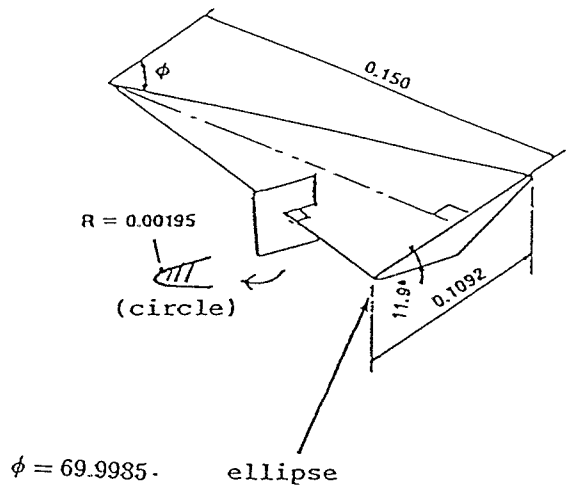


Figure 15. Geometry of the delta wing.

Figure 16. Delta wing. View of the 4 boxes mesh.

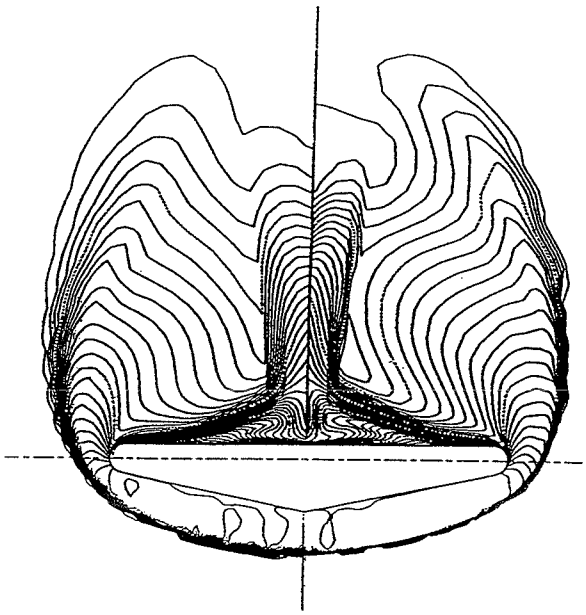

Figure 18. Delta wing. Iso-Mach contours in the final cross section (coarse mesh on the left side and refined one on the right side).

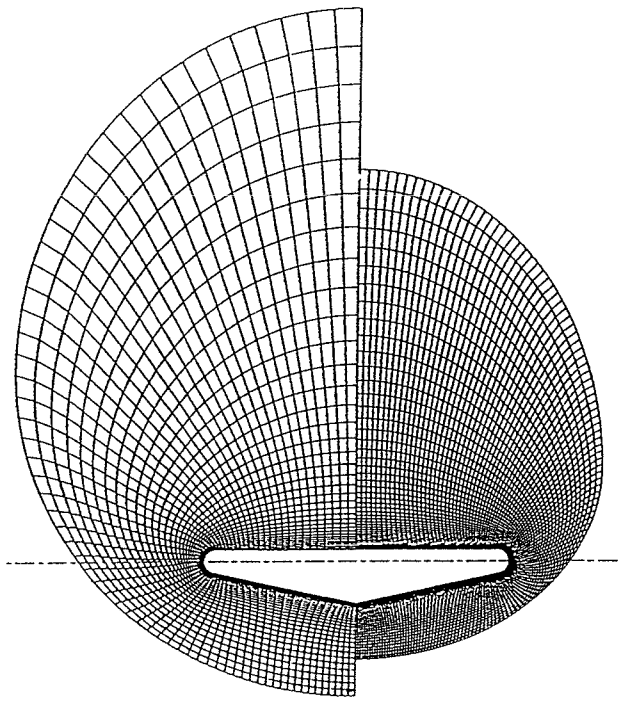

Figure 17. Delta wing. Meshes in the final cross section.

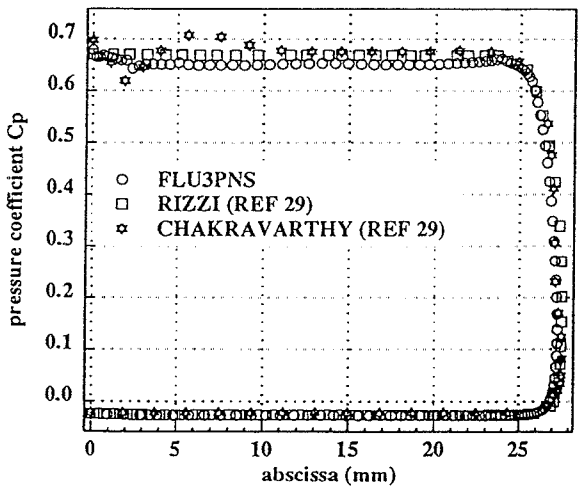


Figure 19. Pressure coefficients on the delta wing in the section z/L = 0.5.

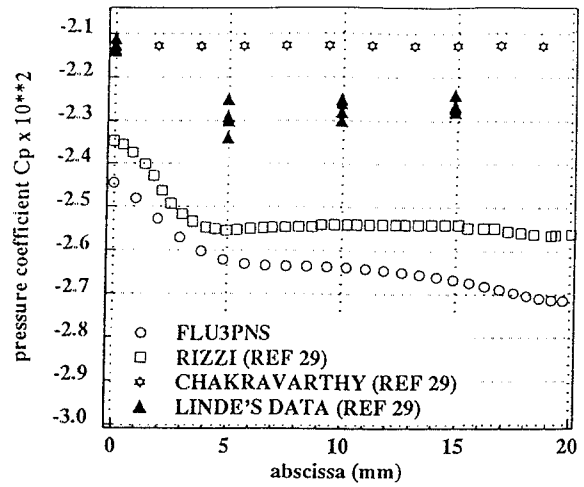


Figure 20. Pressure coefficients on the leeward side of delta wing in the section z/L = 0.5.

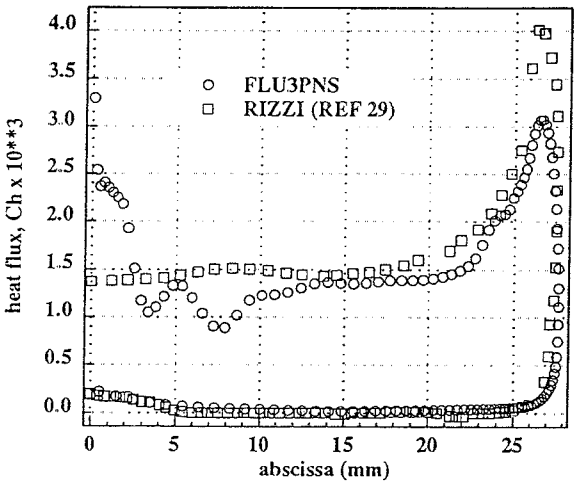


Figure 21. Heat flux on the delta wing in the section z/L = 0.5.

A complete NS solution obtained on the nose of Hermes is followed by four boxes of FLU3PNS (90x50 nodes in each space marching plane), then by a CNS computation for capturing the base flow of the plane ; this result initializes a new FLU3PNS domain for computing the wake. A view of the complete mesh in the meridian plane is presented on Figure 22. We emphasize on the fact that we have used a coarse mesh and inapropriate physical hypothesis of perfect gas ; therefore skin friction and heat flux are neither well predicted nor presented in the present paper. Nevertheless, pressure contours in the meridian plane (Figure 23) show the good compatibility between CNS and PNS boxes. In Figure 24, we detail the velocity vector field in a cross section that corresponds to the winglets of Hermes (it is a FLU3PNS result). The boundary layer is visible on the windward side but the complex structure between plane and wing is not fair at our opinion. In Figure 25 we present isobaric contours in the wake region and Figure 26 shows a three-dimensional view of pressure contours on the surface of Hermes.

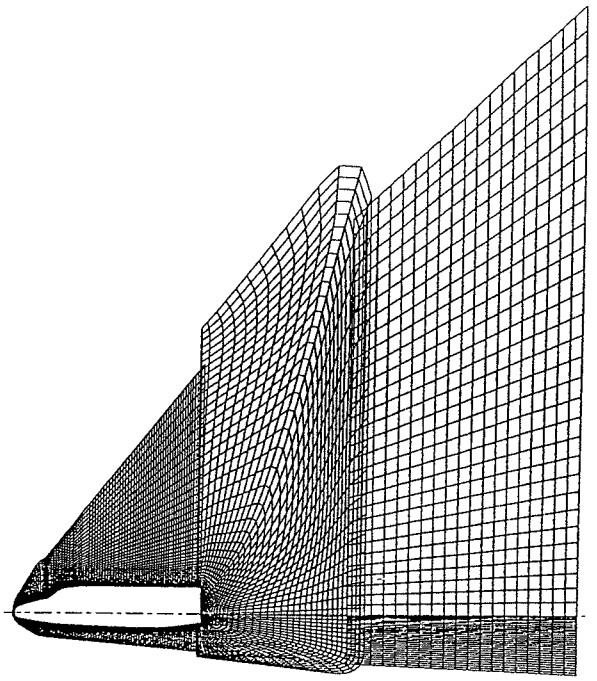

Figure 22. View in the meridian plane of the mesh for coupled CNS and PNS computation around Hermes.

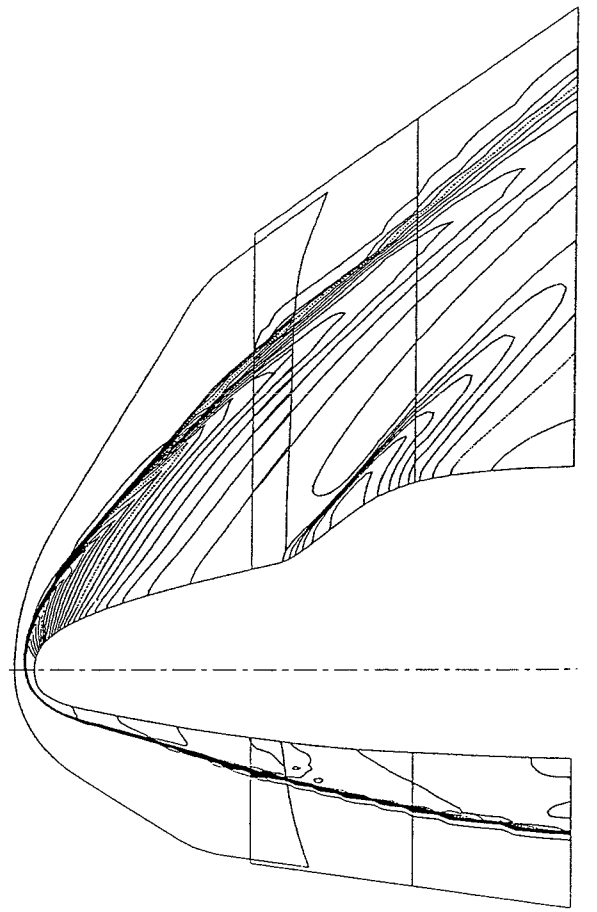

Figure 23. Hermes 0.0 space shuttle. Isobaric lines in the meridian plane.

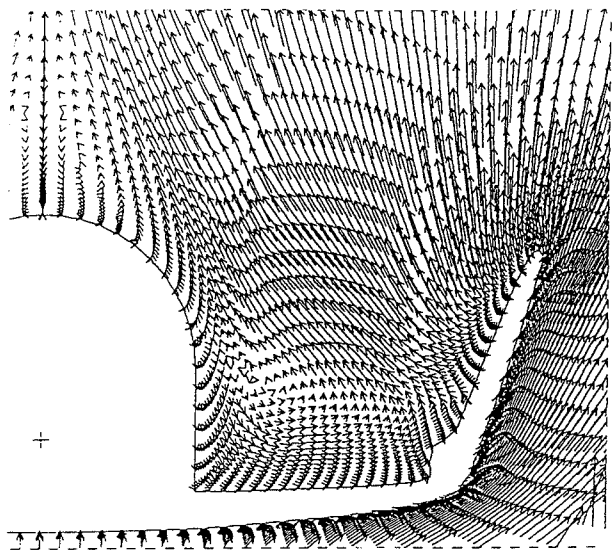

Figure 24. Hermes 0.0 space shuttle. Velocity vector field in the crossflow direction in the winglet region.

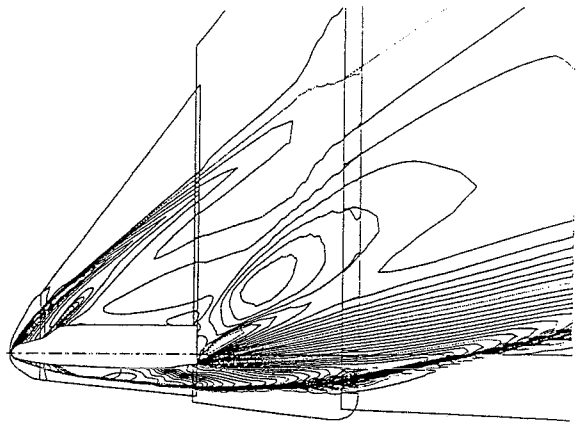

Figure 25. Hermes 0.0 space shuttle. Isobaric lines in the wake region.

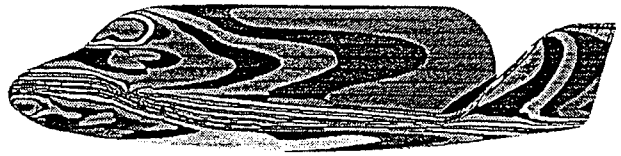

Figure 26. Hermes 0.0 space shuttle. Isobaric lines on the surface of the plane.

## Conclusion

We have presented a finite volume discretization of the TLNS and PNS approximations of the Navier-Stokes equations. The advantage of our formulation is that it gives an extension to an existing Euler code associated with the robust MUSCL upwind scheme and a great flexibility in the choice of the two approximate equations and that it maintains computational efficiency in the PNS case. Several extensions such as real gas effects and implicit scheme are under investigation.

## Acknowledgments

We thank Jean-Jacques Chattot for encouraging us to develop this FLU3PNS solver, François Coron, Hervé Hollanders and Bertrand Mercier for stimulating discussions, Francine Wagner for the boundary layer simulations on the flat plate and Nathalie Drouin for her help in computing Holden's ramp.

## references

1 S.G. Rubin, T.C. Lin, Numerical Methods for Two and Three-Dimensional Viscous Flow Problems, J. Comp. Phys., vol 9, n°2, pp. 339-364, april 1972.

2 S.C. Lubard, W.S. Helliwell, Calculation of the flow on a cone at high angle of attack, AIAA Paper 73-636, AIAA J., vol 12, pp. 965-974, july 1974.

3 Y.C. Vigneron, J.V. Rakich , J.C. Tannehill, Calculations of Supersonic Viscous Flows over Delta Wings with Sharp Subsonic Leading Edges, AIAA Paper 78-1137, july 1978.

4 J.C. Tannehill, E. Venkatapathy, J.V. Rakish, Numerical Solution of Supersonic Viscous Flow over Blunt Delta Wings, AIAA J., vol 20, n° 2, pp. 203-210, february 1982.

5 S.L. Lawrence, J.C. Tannehill, D.S. Chaussee, An Upwind Algorithm for the Parabolized Navier-Stokes Equations, AIAA Paper 86-1117, may 1986.

6 J.C. Tannehill, J.O. Ievalts, S.L. Lawrence, An Upwind Parabolized Navier Stokes Code for Real Gas Flows, AIAA Paper 88-0713, january 1988.

7 J.J.Korte, D.D. Mc Rae, Explicit Upwind Algorithm for the Parabolized Navier-Stokes Equations, AIAA Paper 88-0716, january 1988.

8 O.A. Kandil, A.H. Chung, J.M. Shifflette, Finite Volume Euler and Navier Stokes Solvers for Three-Dimensional and Conical Vortex Flows over Delta Wings, AIAA Paper 87-0041, january 1987.

9 D.Hänel, R. Schwane, An Implicit Flux-Vector Splitting Scheme for the Computation of Viscous Hypersonic Flow, AIAA Paper 89-0274, January 1989.

10 M. Borrel, J.L. Montagné, Numerical Study of a Non-Centered Scheme with Application to Aerodynamics, AIAA Paper 85-1497, 1985.

11 M. Borrel, J.L. Montagné, J. Diet, P. Guillen, J. Lordon, Upwind Scheme for Computing Supersonic Flows Around a Tactical Missile, La Recherche Aerospatiale, n° 1988.2, pp. 43-55, march 1988.

12 C.L. Chang, C.L. Merkle, The Relation between Flux Vector Splitting and Parabolized Schemes, J. Comp. Physics, vol 80, pp. 344-361, 1989.

13 R.W. Newsome, R.W. Walters, J.L. Thomas, An Efficient Iteration Strategy for Upwind-Relaxation Solutions to the Thin-Layer Navier-Stokes Equations, AIAA Paper 87-1113, Honolulu, 1987.

14 J.L. Montagné, calcul tridimensionel de l'interaction d'un jet latéral avec un écoulement supersonique en Navier-Stokes, ONERA Report 20/1408 AY, july 1988.

15 D.A. Anderson, J.C. Tannehill, R.H. Pletcher, Computational Fluid Mechanics and Heat Transfer, Mac Graw Hill, New York, 1984.

16 H. Hollanders, A. Lerat, R. Peyret, Three-Dimensional Calculation of Transonic Viscous Flows by an Implicit Method, AIAA J., vol23, n° 11, pp. 1670-1678, 1985.

17 B. Van Leer , Towards the Ultimate Conservative Scheme V. A Second-Order Sequel to Godunov's Method, J. Comp. Physics, vol 32, pp. 101-136, 1979.

18 G.D. Van Albada, B. Van Leer, W.W. Roberts, A Comparative Study of Computational Methods in Cosmic Gas Dynanics, Astronomy and Astrophysics, vol 108, pp. 76-84, 1982.

19 B.Van Leer, Flux-Vector Splitting for the Euler Equations, in Lecture Notes in Physics n° 170, pp. 507-512, Springer Verlag, 1982.

20 B. Van Leer, J.L. Thomas, P. Roe, R.W. Newsome, A Comparison of Numerical Flux Formulas for the Euler and Navier-Stokes Equations, AIAA Paper 87-1114, 1987.

21 S. Osher, Numerical Solution of Singular Perturbation Problems and Hyperbolic Systems of Conservation Laws, in Math. Studies n° 47, pp. 179-205, North Holland, Amsterdam, 1981.

22 P. Roe, Approximate Riemann Solvers, Parameter Vertors and Difference Schemes, J. Comp. Phys., vol 43, pp. 357-372, 1981.

23 L.B. Schiff, J.L. Steger, Numerical Simulation of Steady Supersonic Flow, AIAA Paper 79-0130, 1979.

24 G. Moulès, Développement du code FLU3PNS, SEGIME report n° 125873, december 1988.

25 H. Hollanders, C. Marmignon, Navier-Stokes High Speed Flow Calculations by an Implicit Non-Centered Finite-Volume Method, AIAA Paper 89-0282, january 1989.

26 F. Noel, Calcul des coefficients de convection et de frottement sur un corps de révolution, Note Technique Sud Aviation, GTP/DE/EAP 75799/68, january1968.

27 R.R. Tracy, Hypersonic Flow Over a Yawed Circular Cone, California Institute of Technology, Aeronautical Laboratories Memorandum n° 69, 1963.

28 M.S. Holden, J.R. Moselle, Theoretical and Experimental Studies of the Shock Wave- Boundary Layer Interaction on Compression Surfaces in Hypersonic Flow, CALSPAN, Buffalo, New York, Report AF-2410-A1, oct 1969.

29 J.A. Desideri, J. Periaux (eds), Proceedings of the Workshop on Hypersonic Flows for Reentry Problems (Part 1, Antibes, january 1990), Springer Verlag, to appear, 1991.